**Supporting Information**

# Isopolymolybdate-induced organic-inorganic hybrid assemblies with copper ions and bichelate-bridging ligands

**Xiu-Li Hao,[a,b] Yuan-Yuan Ma,[a] Yong-Hui Wang,[a] Hong-Ying Zang*[a] and Yang-Guang Li*[a]**

†*Key Laboratory of Polyoxometalate Science of Ministry of Education, Faculty of Chemistry, Northeast Normal University, Renmin Street No. 5268, Changchun, Jilin 130024, P.R. China*

‡*School of Chemical and Biological Engineering, Tai Yuan Science and Technology University, Taiyuan 030012, PR China*

**Contents**

## 1. Additional structural figures for compound 1-7

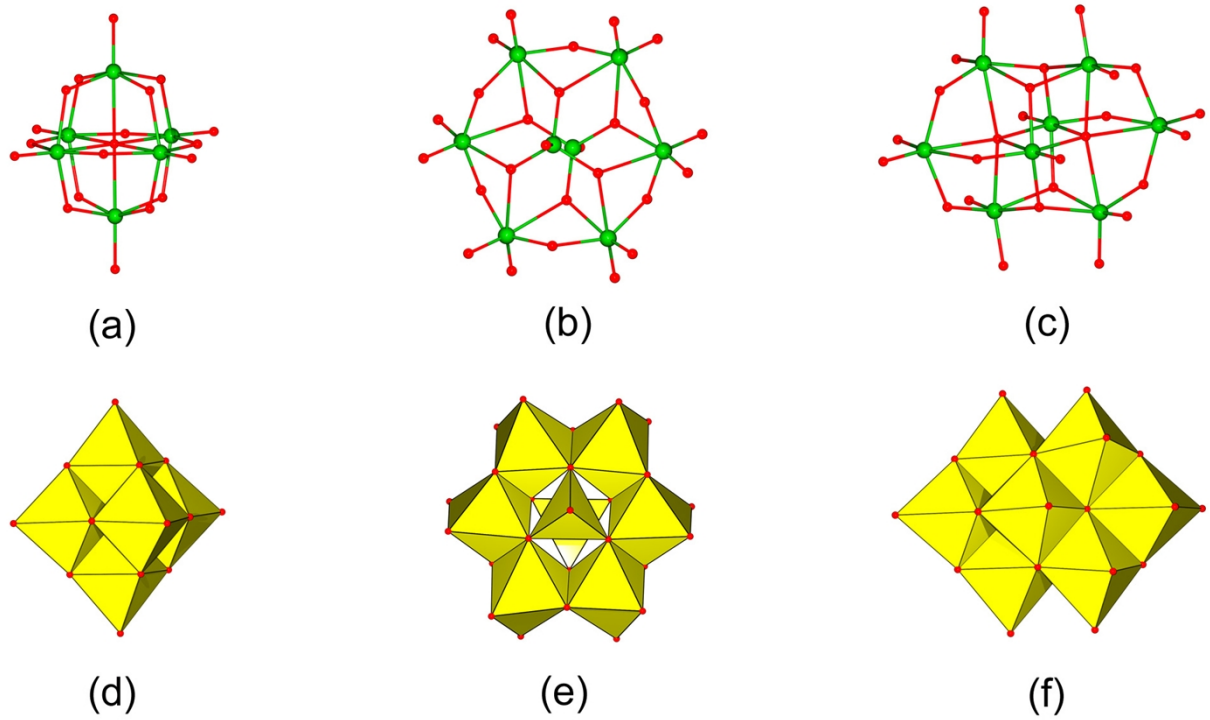


**Figure S1** Ball-and-stick and polyhedral structural view of Lindqvist-type $[Mo_6O_{19}]^{2-}$ **(a) and (d)**, α- $[Mo_8O_{26}]^{4-}$ **(b) and (e )**, and β-$[Mo_8O_{26}]^{4-}$ **(c) and (f)** POM units.

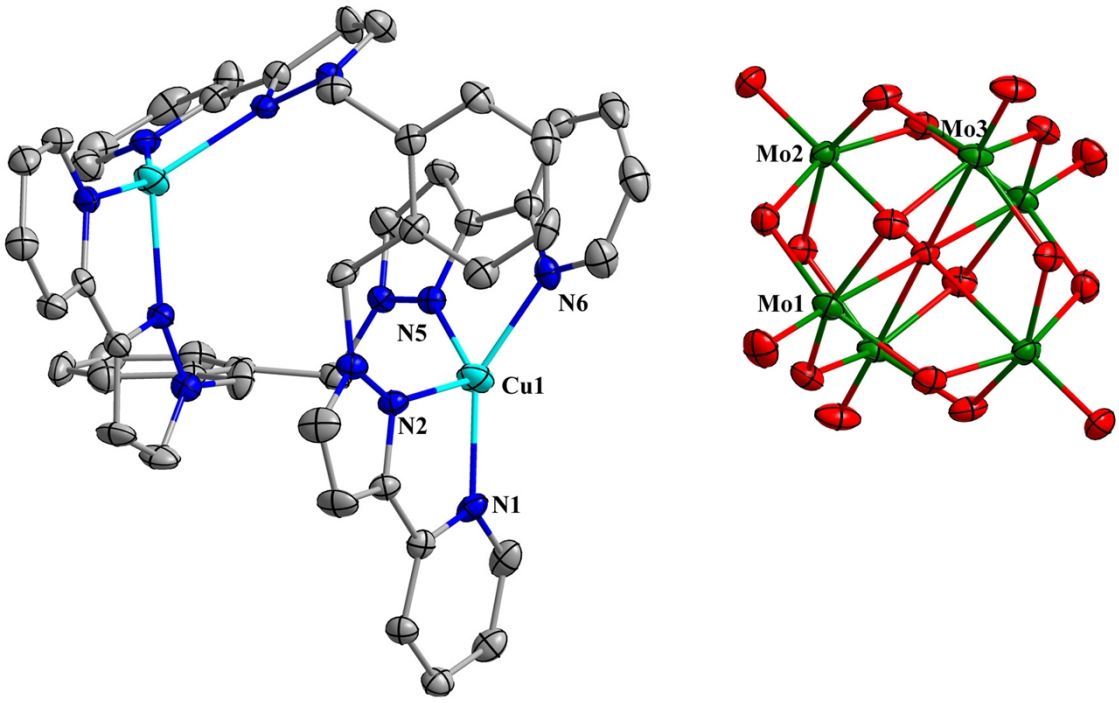


**Figure S2** ORTEP diagram of structure of **1** with thermal ellipsoids at 30% probability displacement. All H atoms are omitted for clarity.

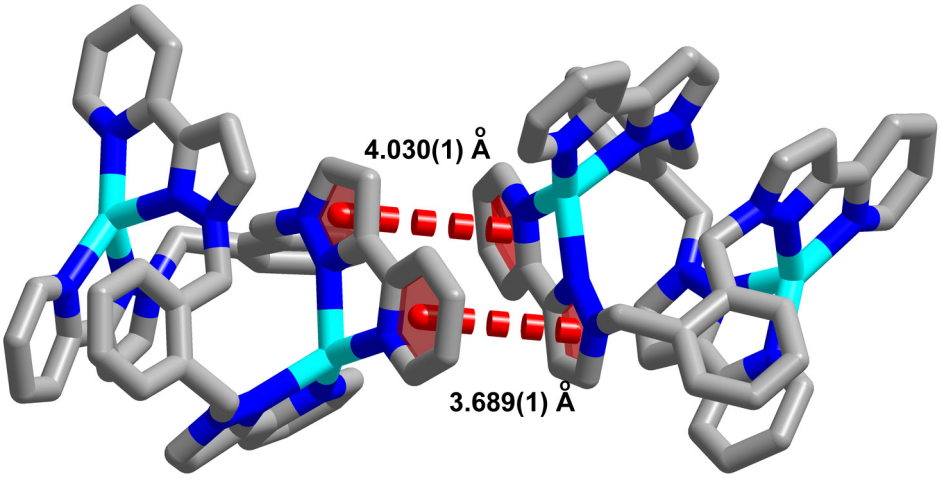


**Figure S3** The typical π…π interactions between two adjacent binuclear $[Cu^{I}_{2}Lo_{2}]^{2+}$ units in **1.** The distances between two adjacent aromatic planes are ca. 3.689(1) Å and ca. 4.030(1) Å.

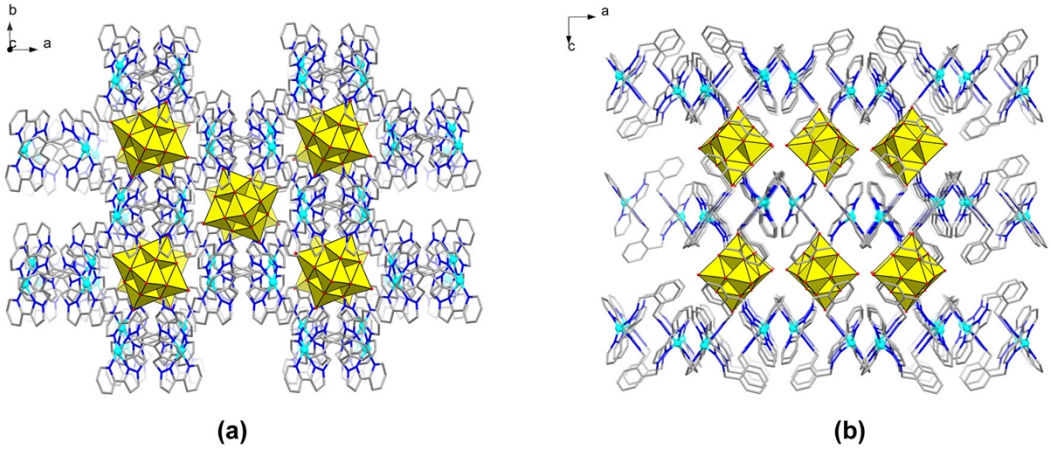


**Figure S4** Packing arrangements of **1** viewed along c **(a)** and *b* **(b)** axis.

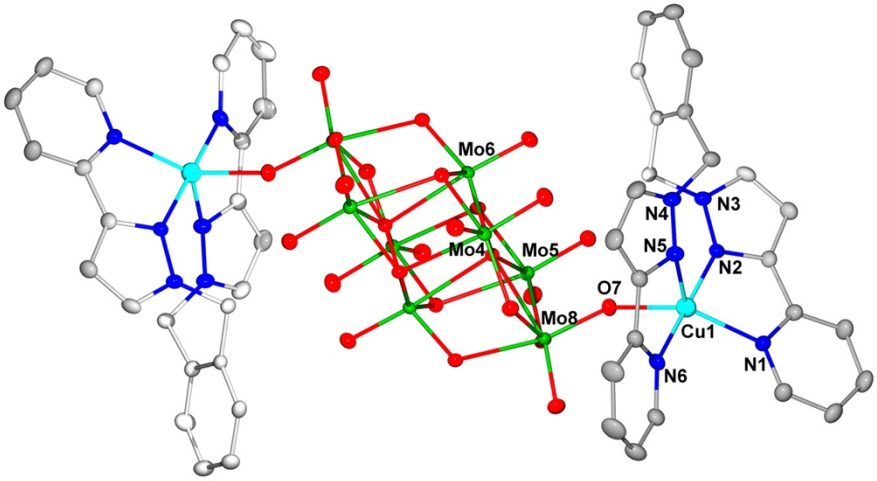


**Figure S5** ORTEP diagram of structure of **2** with thermal ellipsoids at 30% probability displacement. All H atoms are omitted for clarity.

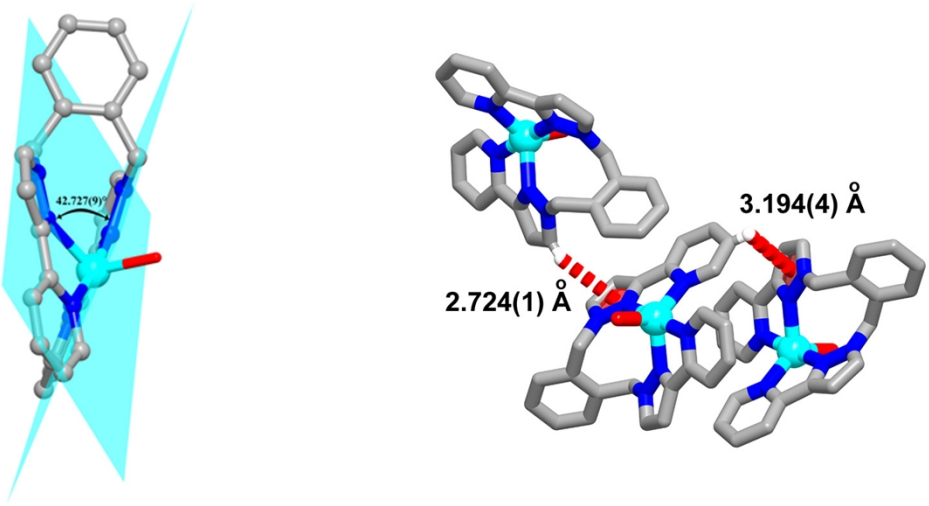


**Figure S6 (a)** The dihedral angel of the two bppmb planes in the [CuL*o*] unit of **2**;
**(b)** The typical C-H…π interactions among adjacent [CuL*o*] units in **2**

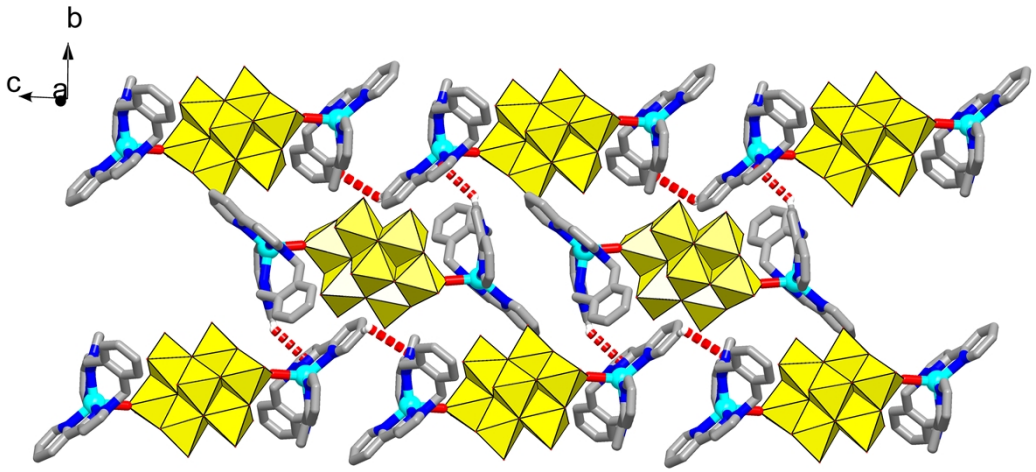


**Figure S7** The 2-D supramolecular layer of **2** in *bc* plane, formed by adjacent hybrid molecules via the weak C-H…π interactions.

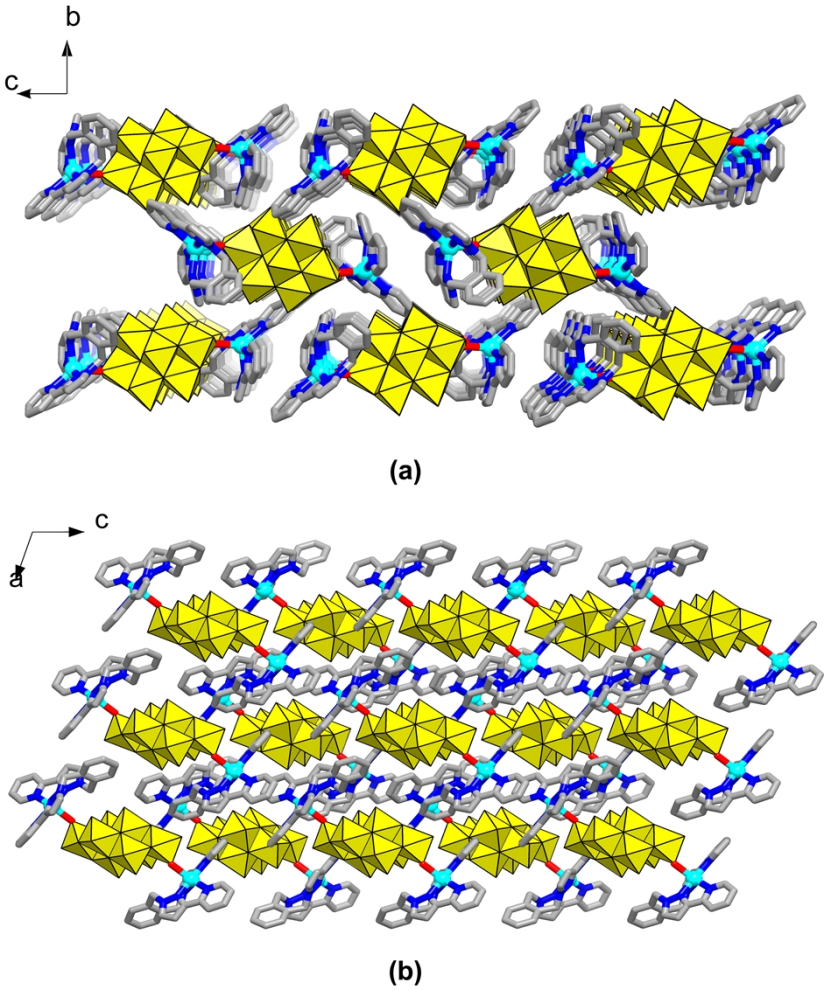


**Figure S8** Packing arrangements of **2** viewed along *a* **(a)** and *b* **(b)** axis.

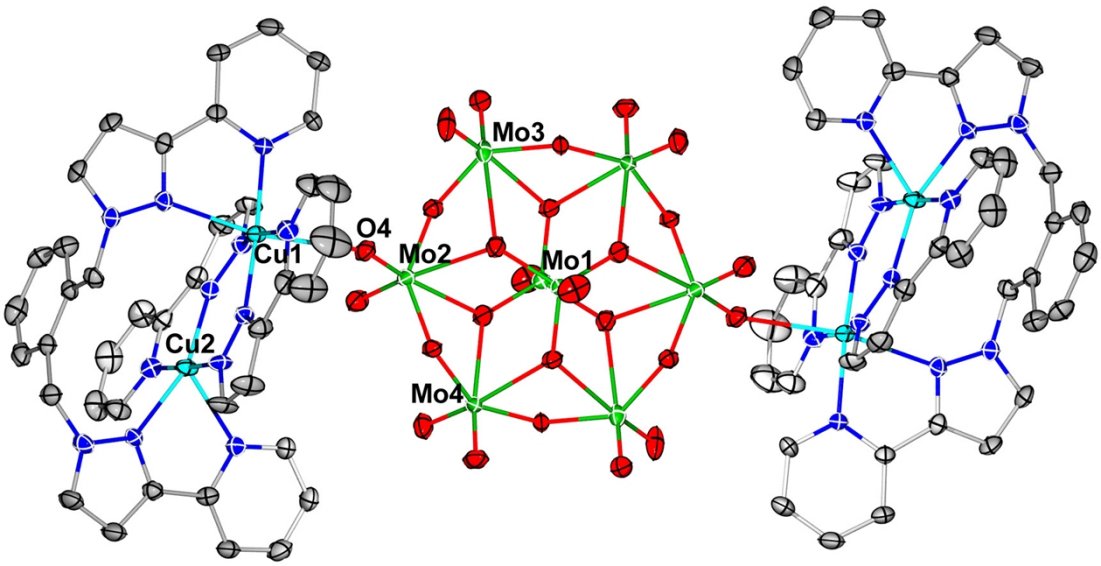


**Figure S9** ORTEP diagram of structure of **3** with thermal ellipsoids at 30% probability displacement. All H atoms are omitted for clarity.

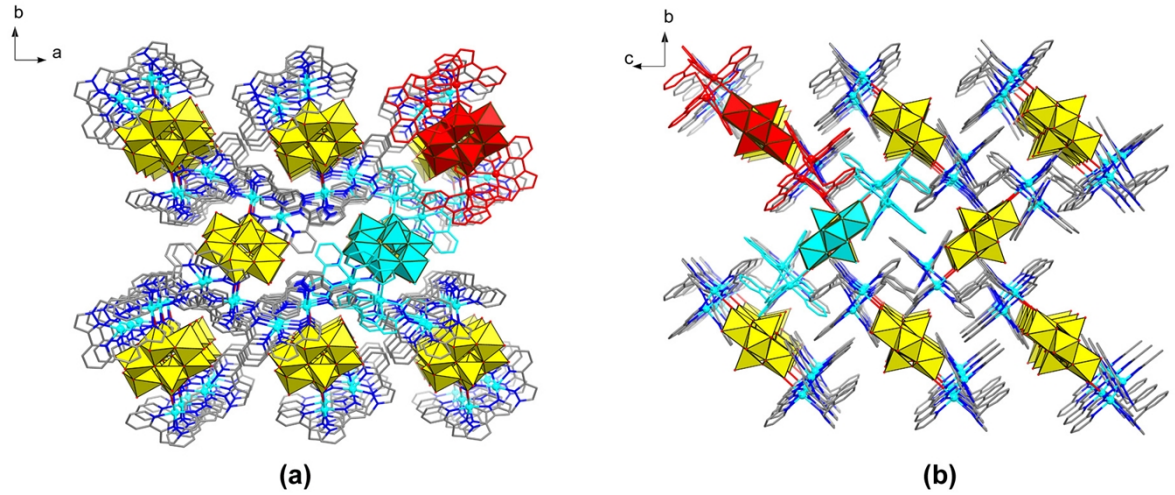


**Figure S10** Packing arrangements of compound **3** viewed along *c* **(a)** and *a* **(b)** axis. The all red and blue hybrid molecules show two kinds of orientations of compound **3** in the packing arrangement.

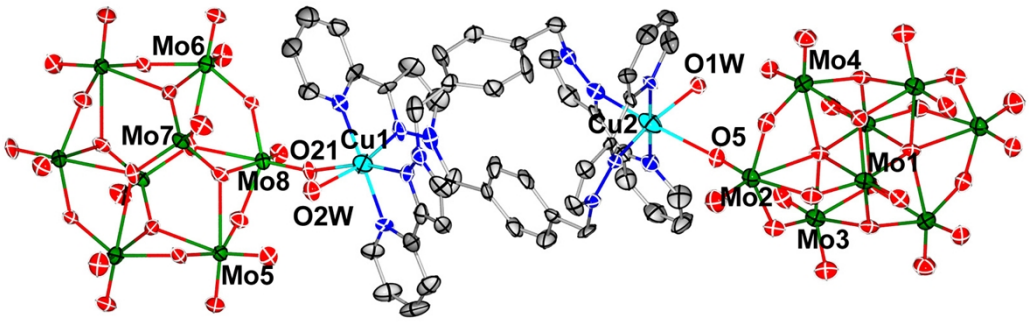


**Figure S11** ORTEP diagram of structure of **4** with thermal ellipsoids at 30% probability displacement. All H atoms are omitted for clarity.

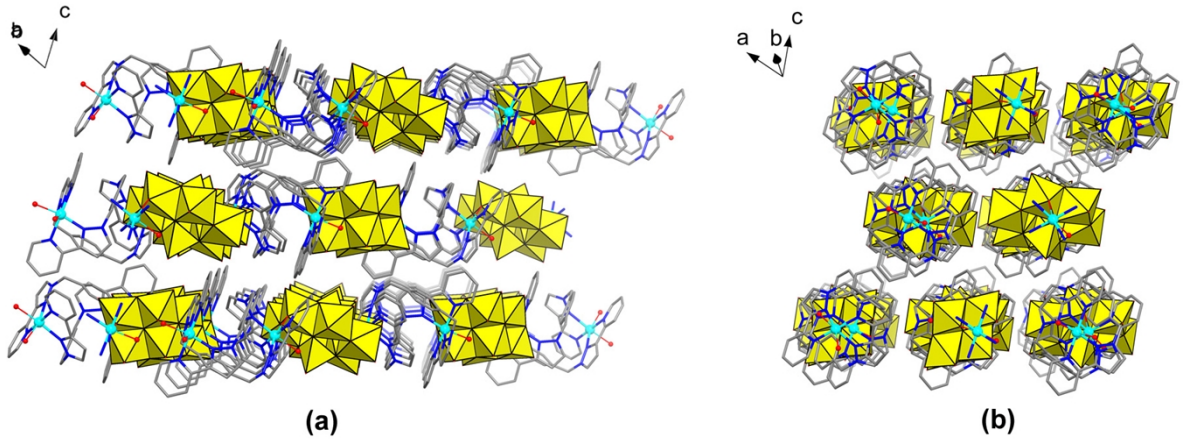


**Figure S12** Packing arrangements of compound **4,** showing that there are no obvious intermolecular interactions among the adjacent hybrid chains.

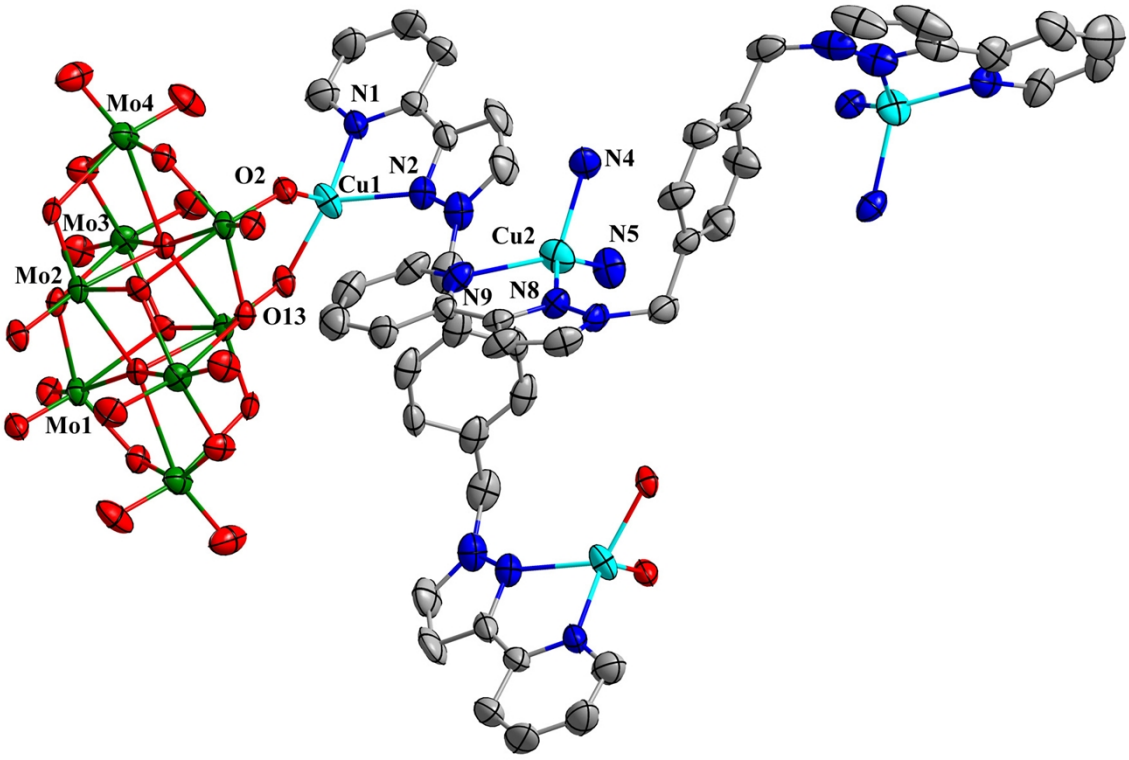


**Figure S13** ORTEP diagram of structure of **5** with thermal ellipsoids at 30% probability displacement. All H atoms are omitted for clarity.

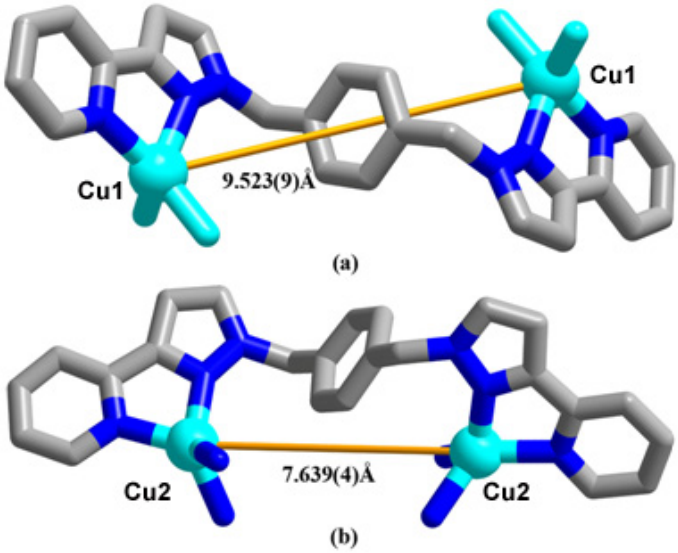


**Figure S14** Configurations of L*p* ligands with **(a)** Cu(1) and **(b)** Cu(2) centers in **5**.

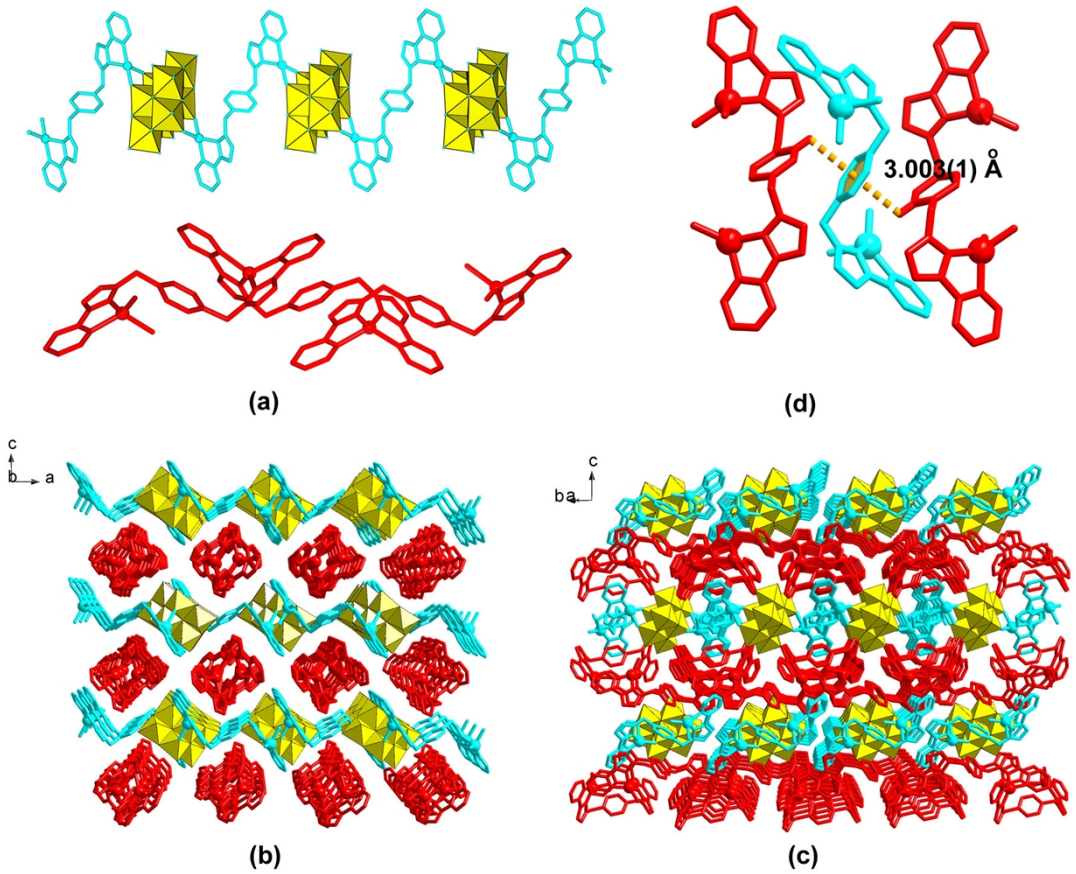


**Figure S15 (a)** View of two kinds of chainlike building blocks in **5**; **(b) and (c)** Packing arrangements of **5**; **(d)** The weak C-H…π interactions between adjacent chains in **5**

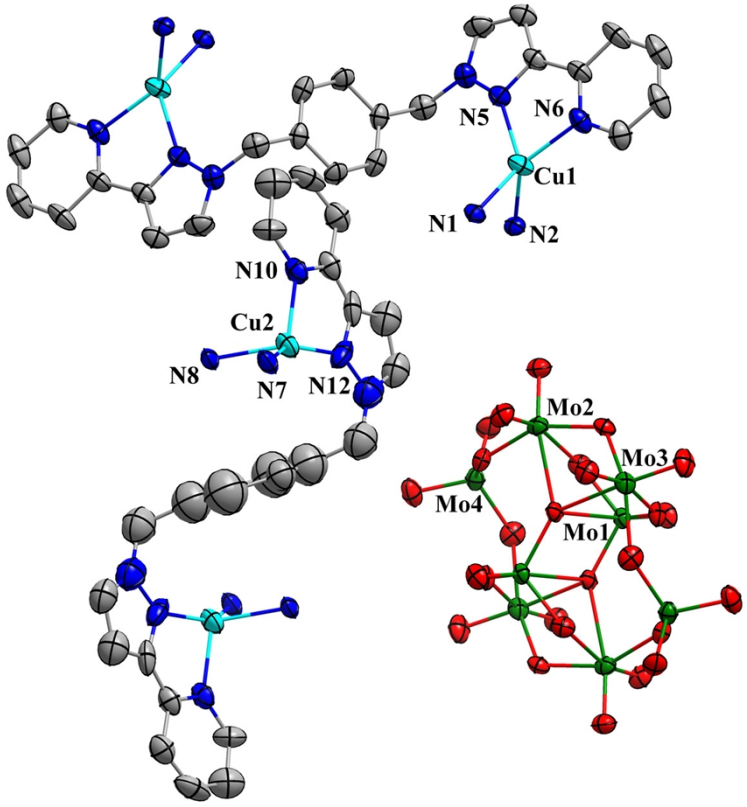


**Figure S16** ORTEP diagram of structure of **6** with thermal ellipsoids at 30% probability displacement. All H atoms are omitted for clarity.

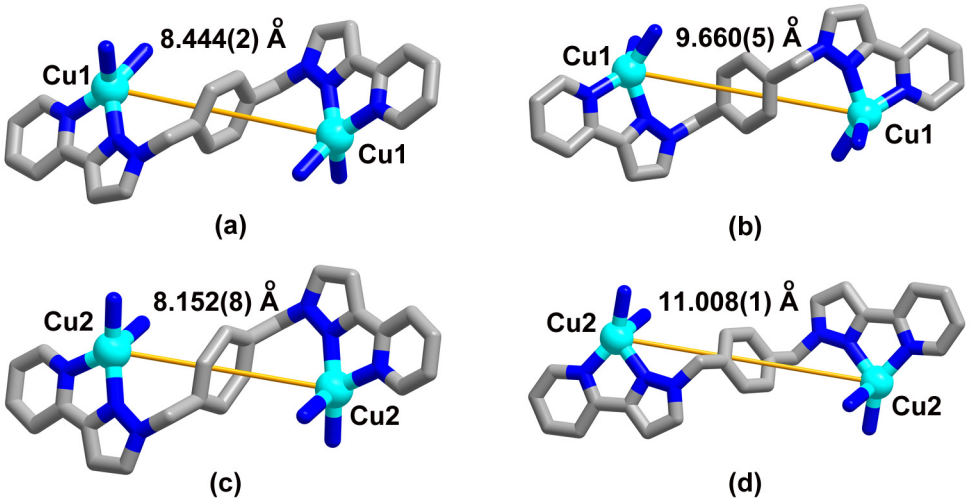


**Figure S17** Four kinds of configurations of L*p* ligands in compound **6, (a) L*p*$^1$, (b) L*p*$^2$, (c) L*p*$^3$** and **(d) L*p*$^4$**

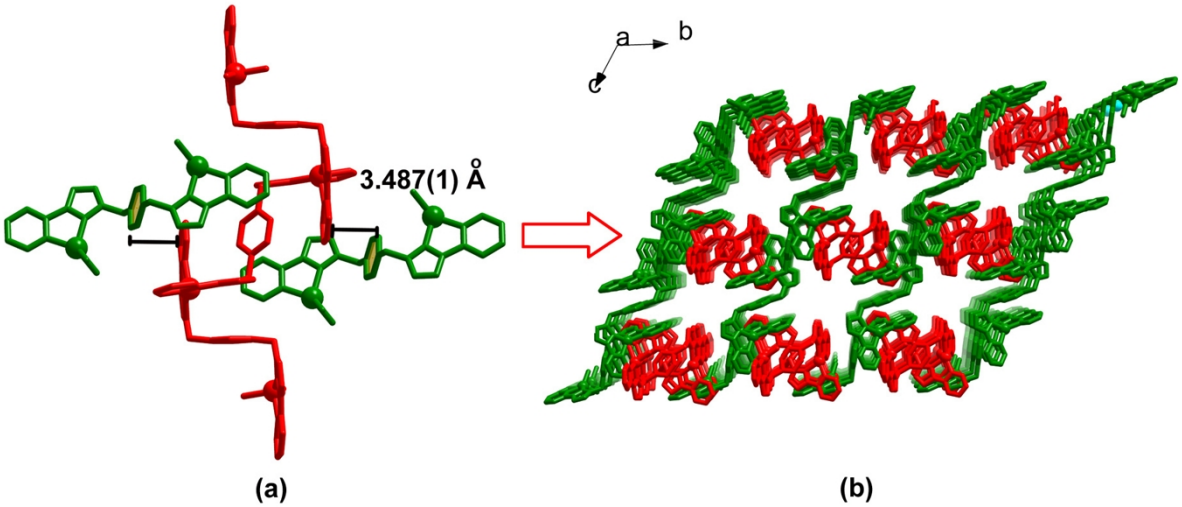


**Figure S18 (a)** The π…π interactions between adjacent chains in **compound 6**. The distance between two adjacent benzene planes is ca. 3.487(1) Å; **(b)** Packing arrangement of two kinds of chains in **6**. The POM units in the cavities of 3-D supramolecular framework are omitted for clarity.

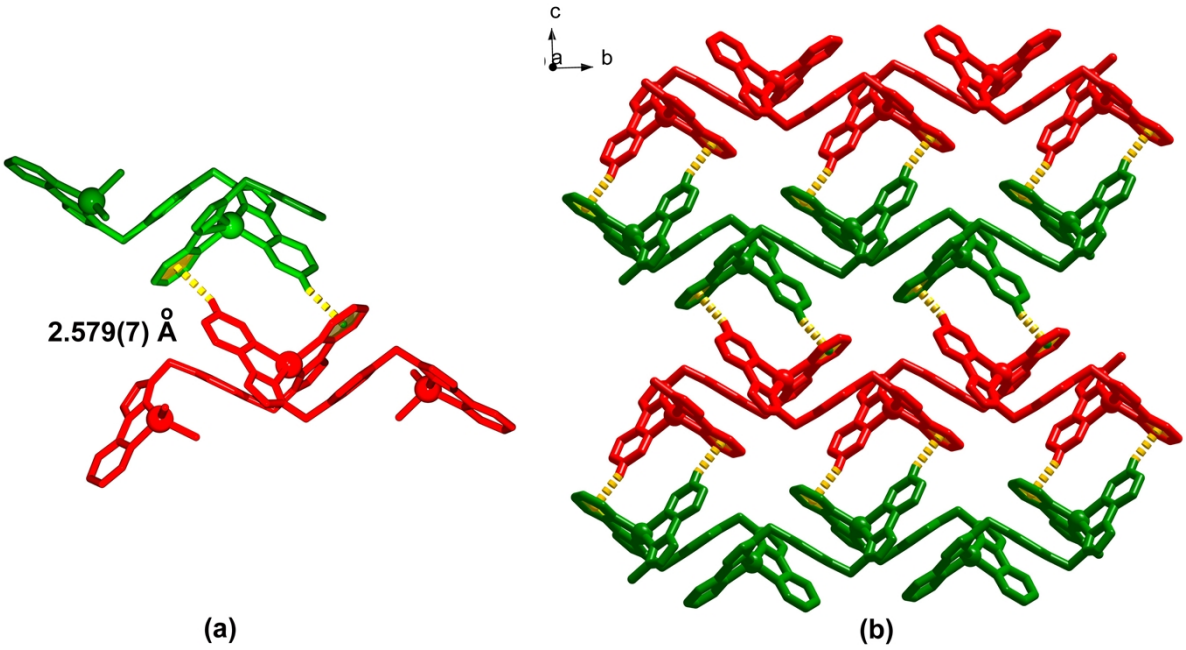


**Figure S19** The C-H…π intermolecular interactions between adjacent chains on the *bc* plane

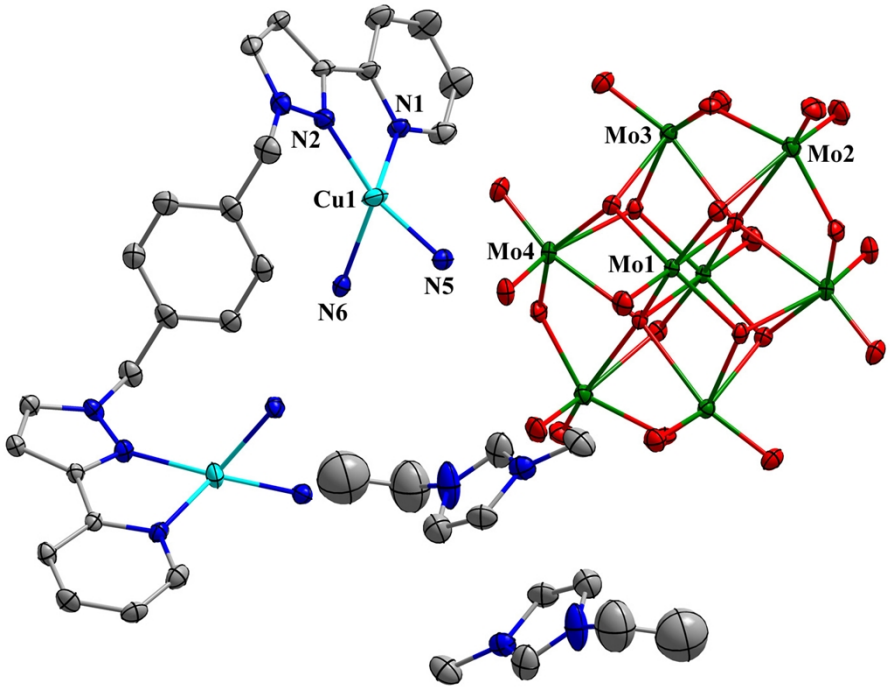


**Figure S20** ORTEP diagram of structure of **7** with thermal ellipsoids at 30% probability displacement. All H atoms are omitted for clarity.

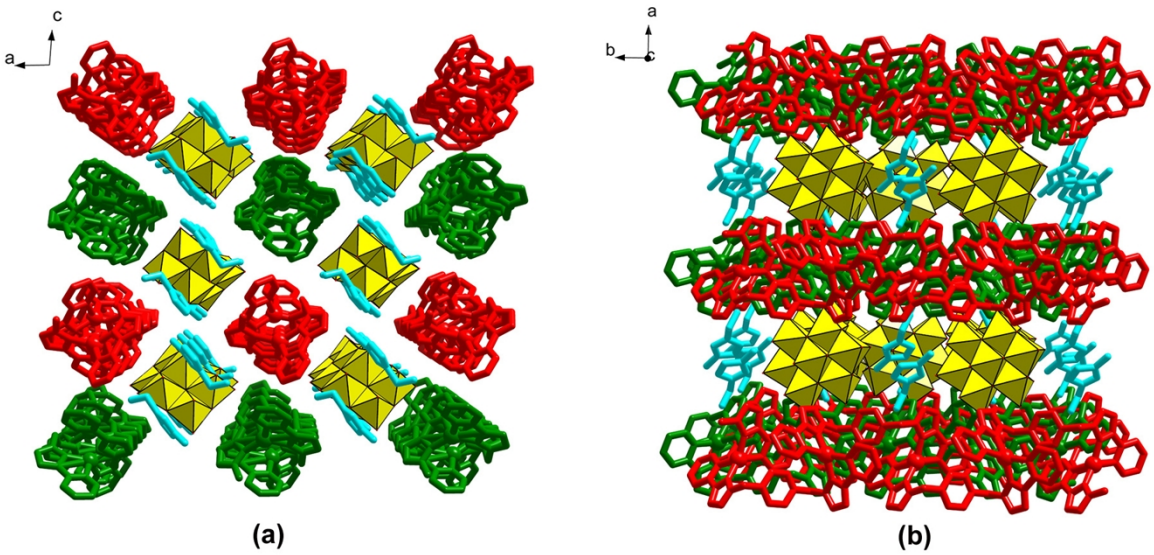


**Figure S21** Packing arrangements of compound **7** viewed along **(a)** *b* axis and **(b)** *c* axis

**2.** Selected bond lengths and angles for compounds **1-7**

**Table S1**. Selected bond lengths (Å) and angles (deg) of **1**.

| | | | |
|---|---|---|---|
| Cu(1)-N(1) | 2.021(5) | Cu(1)-N(6)#1 | 2.029(5) |
| Cu(1)-N(5)#1 | 2.107(5) | Cu(1)-N(2) | 2.122(5) |
| N(1)-Cu(1)-N(6)#1 | 146.5(2) | N(1)-Cu(1)-N(5)#1 | 122.46(19) |
| N(6)#1-Cu(1)-N(5)#1 | 80.7(2) | N(1)-Cu(1)-N(2) | 80.82(19) |
| N(6)#1-Cu(1)-N(2) | 110.30(19) | N(5)#1-Cu(1)-N(2) | 119.34(19) |

Symmetry transformations used to generate equivalent atoms: #1 -x,y,-z+1/2 #2 -x+1,-y+1,-z

**Table S2**. Selected bond lengths (Å) and angles (deg) of **2**.

| | | | |
|---|---|---|---|
| Cu(1)-N(2) | 1.957(3) | Cu(1)-N(6) | 1.987(3) |
| Cu(1)-O(7) | 2.063(2) | Cu(1)-N(1) | 2.085(3) |
| Cu(1)-N(5) | 2.140(3) | N(2)-Cu(1)-N(6) | 176.24(13) |
| N(2)-Cu(1)-O(7) | 94.04(11) | N(6)-Cu(1)-O(7) | 88.52(11) |
| N(2)-Cu(1)-N(1) | 80.18(12) | N(6)-Cu(1)-N(1) | 99.94(13) |
| O(7)-Cu(1)-N(1) | 135.16(12) | N(2)-Cu(1)-N(5) | 96.62(12) |
| N(6)-Cu(1)-N(5) | 80.09(13) | O(7)-Cu(1)-N(5) | 103.22(12) |
| N(1)-Cu(1)-N(5) | 121.58(12) | | |

Symmetry transformations used to generate equivalent atoms: #1 -x+2,-y,-z+1

**Table S3**. Selected bond lengths (Å) and angles (deg) of **3**.

| | | | |
|---|---|---|---|
| Cu(1)-N(8) | 1.960(5) | Cu(1)-N(12) | 1.974(5) |
| Cu(1)-N(6) | 2.042(4) | Cu(1)-N(7) | 2.059(5) |
| Cu(1)-N(5) | 2.315(4) | Cu(2)-N(9) | 1.951(5) |
| Cu(2)-N(11) | 1.964(4) | Cu(2)-N(10) | 2.040(5) |
| Cu(2)-N(2) | 2.115(4) | Cu(2)-N(1) | 2.221(5) |
| Cu(1)-O(4) | 2.594(0) | | |
| N(8)-Cu(1)-N(12) | 96.47(19) | N(8)-Cu(1)-N(6) | 168.8(2) |
| N(12)-Cu(1)-N(6) | 93.19(19) | N(8)-Cu(1)-N(7) | 80.7(2) |
| N(12)-Cu(1)-N(7) | 168.34(19) | N(6)-Cu(1)-N(7) | 90.9(2) |
| N(8)-Cu(1)-N(5) | 97.94(18) | N(12)-Cu(1)-N(5) | 92.77(18) |
| N(6)-Cu(1)-N(5) | 75.89(17) | N(7)-Cu(1)-N(5) | 98.82(18) |
| O(4)-Cu(1)-N(5) | 169.05(41) | O(4)-Cu(1)-N(6) | 93.16(72) |
| O(4)-Cu(1)-N(7) | 81.77(72) | O(4)-Cu(1)-N(8) | 92.98(32) |
| O(4)-Cu(1)-N(12) | 87.06(82) | N(9)-Cu(2)-N(11) | 96.67(19) |
| N(9)-Cu(2)-N(10) | 177.1(2) | N(11)-Cu(2)-N(10) | 80.99(19) |
| N(9)-Cu(2)-N(2) | 90.52(18) | N(11)-Cu(2)-N(2) | 159.95(18) |
| N(10)-Cu(2)-N(2) | 91.15(18) | N(9)-Cu(2)-N(1) | 95.53(18) |
| N(11)-Cu(2)-N(1) | 121.95(18) | N(10)-Cu(2)-N(1) | 87.19(18) |
| N(2)-Cu(2)-N(1) | 75.64(17) | | |

Symmetry transformations used to generate equivalent atoms: #1 -x,-y+1,-z

**Table S4**. Selected bond lengths (Å) and angles (deg) of **4**.

| | | | |
|---|---|---|---|
| Cu(1)-N(12) | 1.956(9) | Cu(1)-N(1) | 1.969(10) |
| Cu(1)-O(2W) | 2.103(9) | Cu(1)-N(2) | 2.106(11) |
| Cu(1)-N(11) | 2.283(11) | Cu(1)-O(21) | 2.317(8) |
| Cu(2)-N(7) | 1.977(10) | Cu(2)-N(6) | 2.010(9) |
| Cu(2)-N(5) | 2.030(10) | Cu(2)-O(1W) | 2.029(8) |
| Cu(2)-N(8) | 2.355(11) | Cu(2)-O(5) | 2.479(7) |
| N(12)-Cu(1)-N(1) | 178.9(4) | N(12)-Cu(1)-O(2W) | 87.5(4) |
| N(1)-Cu(1)-O(2W) | 91.9(4) | N(12)-Cu(1)-N(2) | 99.9(4) |
| N(1)-Cu(1)-N(2) | 80.4(4) | O(2W)-Cu(1)-N(2) | 165.3(4) |
| N(12)-Cu(1)-N(11) | 77.9(4) | N(1)-Cu(1)-N(11) | 103.0(4) |
| O(2W)-Cu(1)-N(11) | 85.1(4) | N(2)-Cu(1)-N(11) | 108.8(4) |
| N(12)-Cu(1)-O(21) | 92.6(3) | N(1)-Cu(1)-O(21) | 86.3(4) |
| O(2W)-Cu(1)-O(21) | 83.1(3) | N(2)-Cu(1)-O(21) | 83.9(4) |
| N(11)-Cu(1)-O(21) | 165.2(4) | N(7)-Cu(2)-N(6) | 179.9(5) |
| N(7)-Cu(2)-N(5) | 99.1(4) | N(6)-Cu(2)-N(5) | 80.8(4) |
| N(7)-Cu(2)-O(1W) | 89.8(4) | N(6)-Cu(2)-O(1W) | 90.3(4) |
| N(5)-Cu(2)-O(1W) | 164.3(4) | N(7)-Cu(2)-N(8) | 76.7(4) |
| N(6)-Cu(2)-N(8) | 103.3(4) | N(5)-Cu(2)-N(8) | 103.6(4) |
| O(1W)-Cu(2)-N(8) | 90.9(4) | O(5)-Cu(2)-N(6) | 85.4(2) |
| O(5)-Cu(2)-N(5) | 86.2(7) | O(5)-Cu(2)-N(7) | 94.4(8) |
| O(5)-Cu(2)-N(8) | 167.3(1) | O(5)-Cu(2)-O(1W) | 80.3(3) |

Symmetry transformations used to generate equivalent atoms: -x+1,-y,-z+1 #2 -x,-y+3,-z

**Table S5**. Selected bond lengths (Å) and angles (deg) of **5**.

| | | | |
|---|---|---|---|
| Cu(1)-O(13) | 1.929(6) | Cu(1)-N(1) | 2.003(10) |
| Cu(1)-O(2)#1 | 2.063(7) | Cu(1)-N(2) | 2.107(9) |
| Cu(2)-N(8) | 1.974(8) | Cu(2)-N(5) | 2.011(9) |
| Cu(2)-N(4) | 2.038(10) | Cu(2)-N(9) | 2.107(10) |
| O(13)-Cu(1)-N(1) | 136.8(3) | O(13)-Cu(1)-O(2)#1 | 92.7(3) |
| N(1)-Cu(1)-O(2)#1 | 121.6(3) | O(13)-Cu(1)-N(2) | 124.5(3) |
| N(1)-Cu(1)-N(2) | 81.4(4) | O(2)#1-Cu(1)-N(2) | 94.5(3) |
| N(8)-Cu(2)-N(5) | 132.5(4) | N(8)-Cu(2)-N(4) | 126.0(4) |
| N(5)-Cu(2)-N(4) | 81.4(5) | N(8)-Cu(2)-N(9) | 80.5(3) |
| N(5)-Cu(2)-N(9) | 123.2(4) | N(4)-Cu(2)-N(9) | 118.6(4) |

Symmetry transformations used to generate equivalent atoms: #1 -x,-y+2,-z #2 -x-1/2,-y+3/2,-z #3 -x-1/2,y+1/2,-z+1/2 #4 -x-1/2,y-1/2,-z+1/2 #5 -x,y,-z+1/2

**Table S6**. Selected bond lengths (Å) and angles (deg) of **6**.

| | | | |
|---|---|---|---|
| Cu(1)-N(6) | 2.023(7) | Cu(1)-N(2) | 2.047(7) |
| Cu(1)-N(1) | 2.079(6) | Cu(1)-N(5) | 2.086(7) |
| Cu(2)-N(7) | 2.008(9) | Cu(2)-N(12) | 2.056(7) |
| Cu(2)-N(8) | 2.068(7) | Cu(2)-N(10) | 2.076(9) |
| N(6)-Cu(1)-N(2) | 133.4(3) | N(6)-Cu(1)-N(1) | 127.9(3) |

| | | | |
|---|---|---|---|
| N(2)-Cu(1)-N(1) | 80.3(3) | N(6)-Cu(1)-N(5) | 81.2(3) |
| N(2)-Cu(1)-N(5) | 111.6(3) | N(1)-Cu(1)-N(5) | 128.1(3) |
| N(7)-Cu(2)-N(12) | 145.8(3) | N(7)-Cu(2)-N(8) | 82.1(3) |
| N(12)-Cu(2)-N(8) | 122.5(3) | N(7)-Cu(2)-N(10) | 123.6(3) |
| N(12)-Cu(2)-N(10) | 77.4(3) | N(8)-Cu(2)-N(10) | 102.6(3) |

Symmetry transformations used to generate equivalent atoms: #1 -x,-y-1,-z #2 -x+1,-y,-z #3 -x+2,-y,-z+1 #4 -x,-y+1,-z+1 #5 -x+1,-y+1,-z+1

**Table S7**. Selected bond lengths (Å) and angles (deg) of **7**.

| | | | |
|---|---|---|---|
| Cu(1)-N(2) | 2.005(5) | Cu(1)-N(5)#1 | 2.021(5) |
| Cu(1)-N(6)#1 | 2.091(5) | Cu(1)-N(1) | 2.120(5) |
| N(2)-Cu(1)-N(5)#1 | 136.7(2) | N(2)-Cu(1)-N(6)#1 | 130.0(2) |
| N(5)#1-Cu(1)-N(6)#1 | 80.5(2) | N(2)-Cu(1)-N(1) | 79.5(2) |
| N(5)#1-Cu(1)-N(1) | 121.7(2) | N(6)#1-Cu(1)-N(1) | 111.4(2) |

Symmetry transformations used to generate equivalent atoms: #1 -x,y+1/2,-z+1/2 #2 -x+1,-y+1,-z #3 -x,y-1/2,-z+1/2

**3.** Additional measurements for compounds **1-7**

3.1 Photocatalysis properties

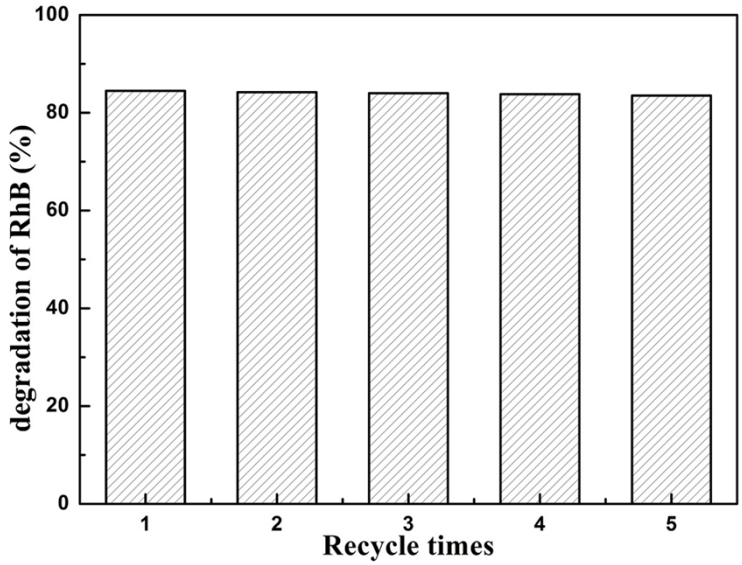


**Figure S22** The recycle times on the RhB degradation with compound **4** as catalyst.

**3.2** IR spectra

In the IR spectrum of **1**, the characteristic peaks at 800 and 955 $cm^{-1}$ are attributed to the *v*(Mo-O-Mo) and *v*(Mo=O) of the $[Mo_6O_{19}]^{2-}$ polyanions, respectively (Fig. S23). The IR spectra of compounds **2-7** show characteristic peaks of the polyoxoanion $[Mo_8O_{26}]^{4-}$ in the range of 660-953 $cm^{-1}$ for **2**, 673-939 $cm^{-1}$ for **3**, 657-945 $cm^{-1}$ for **4,** 642-944 $cm^{-1}$ for **5**, 659-916 $cm^{-1}$ for **6** and 659-947 $cm^{-1}$ for 7, which are ascribed to the vibrations of *v*(Mo-$O_t$) and *v*(Mo-O-Mo) (Fig. S24- S29). In addition, for all compounds, the peaks at ca. 3110 $cm^{-1}$ are attributed to the vibrations of the *v*(C-H) in phenyl, pyrazole and pyridyl rings of L*o* and L*p* ligand. Peaks in the regions of 1645-1434 $cm^{-1}$ may belong to the vibrations of the *v*(C=C), *v*(C=N) and *v*(C=N) in phenyl, pyrazole and pyridyl rings of L*o* and L*p* ligand in **1-7**. The peaks at ca. 3440 $cm^{-1}$ are attributed to the vibrations of *v*($H_2O$).

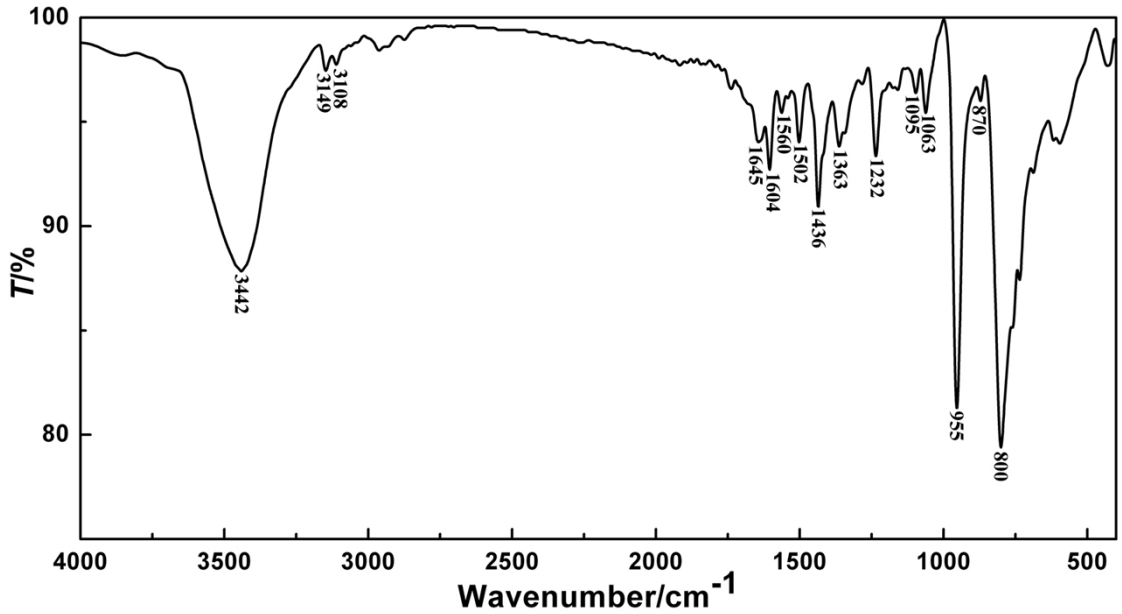


**Figure S23** IR spectrum of compound **1**.

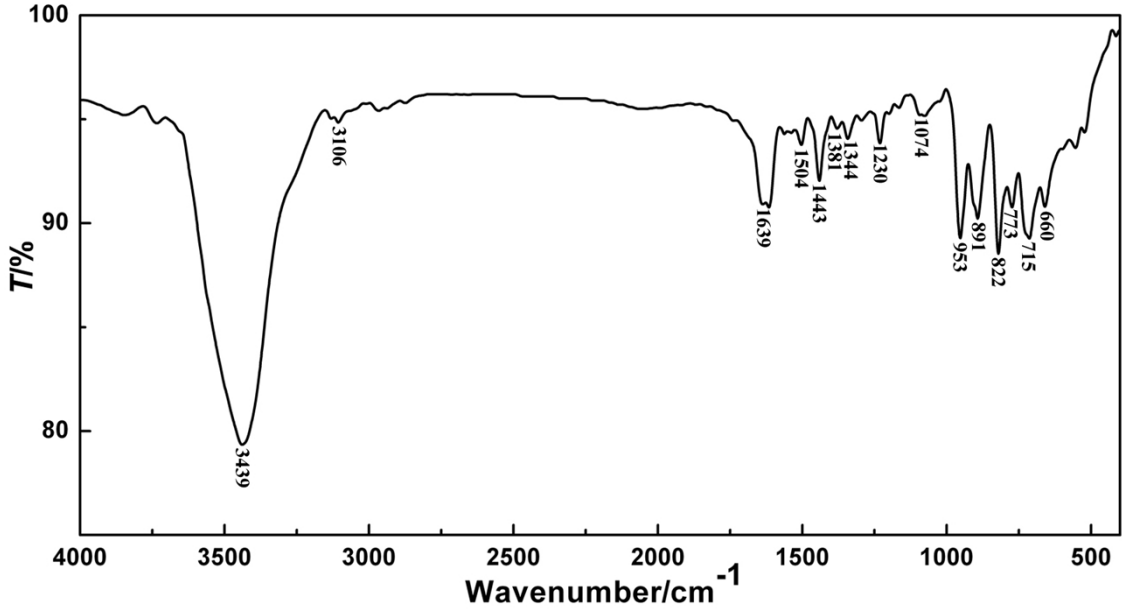


**Figure S24** IR spectrum of compound **2**.

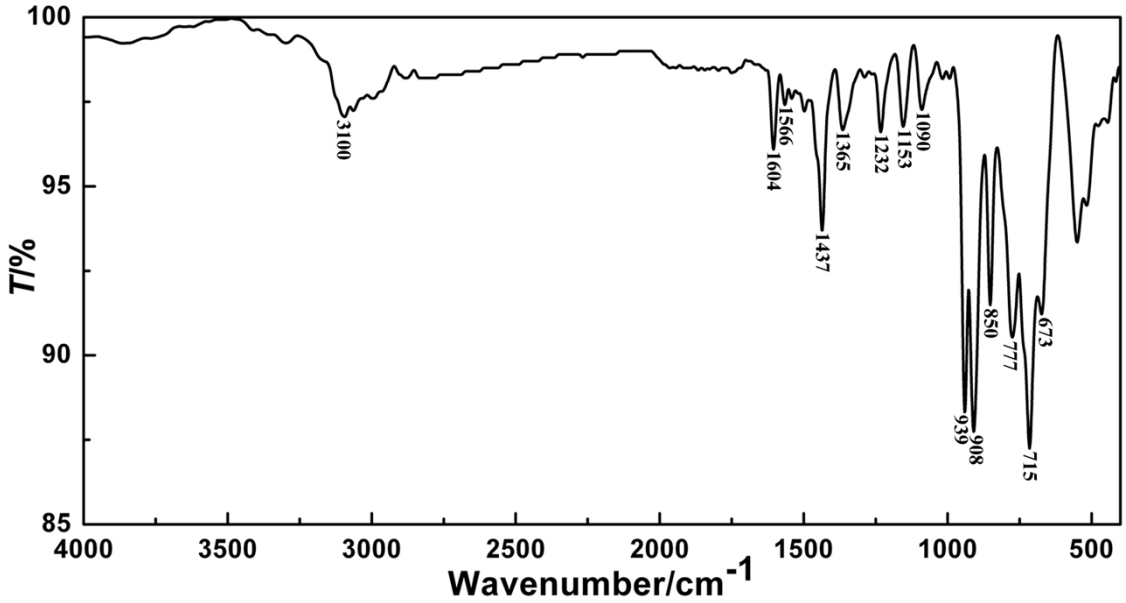


**Figure S25** IR spectrum of compound **3**.

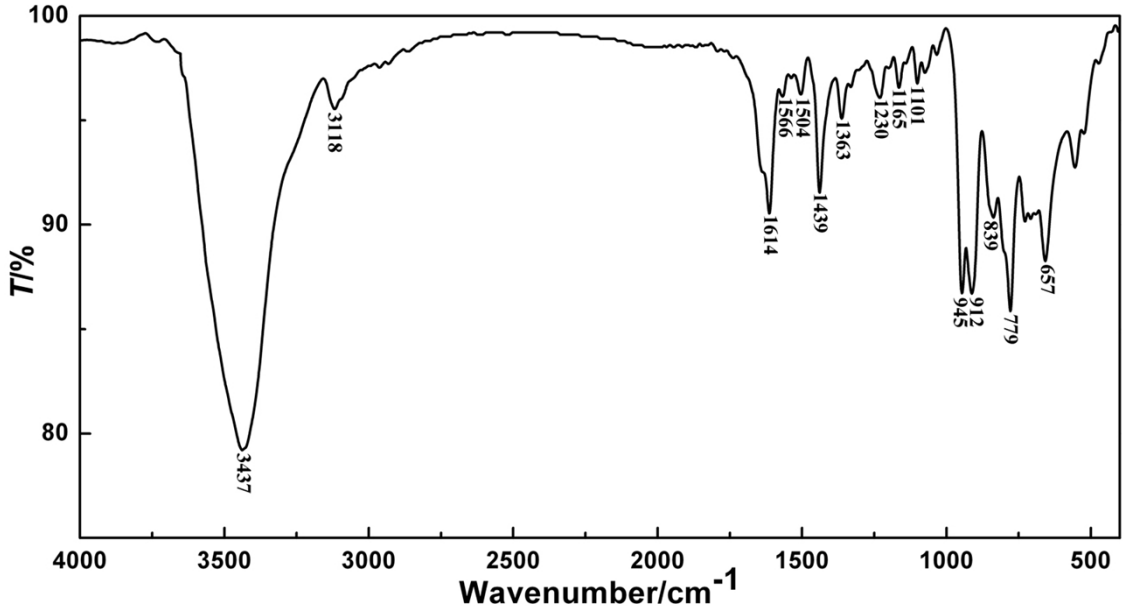


**Figure S26** IR spectrum of compound **4**.

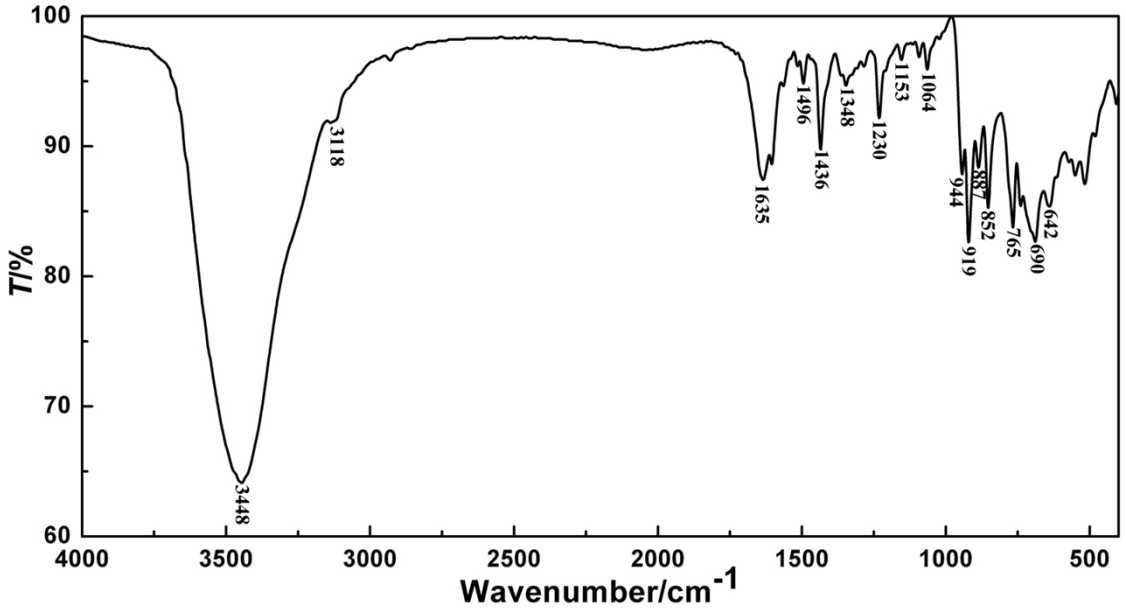


**Figure S27** IR spectrum of compound **5**.

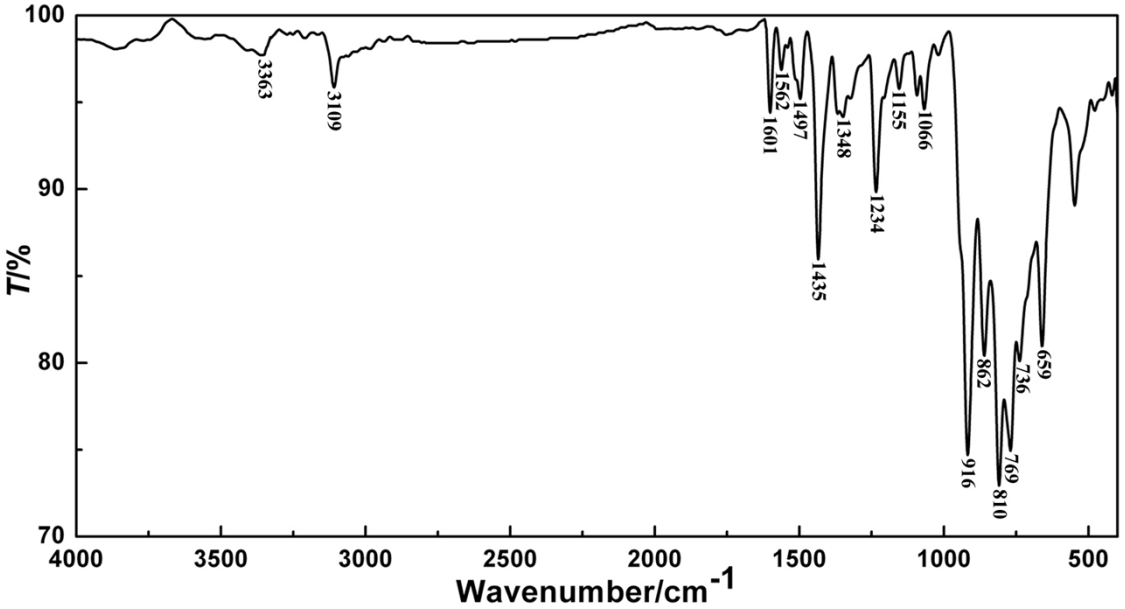


**Figure S28** IR spectrum of compound **6**.

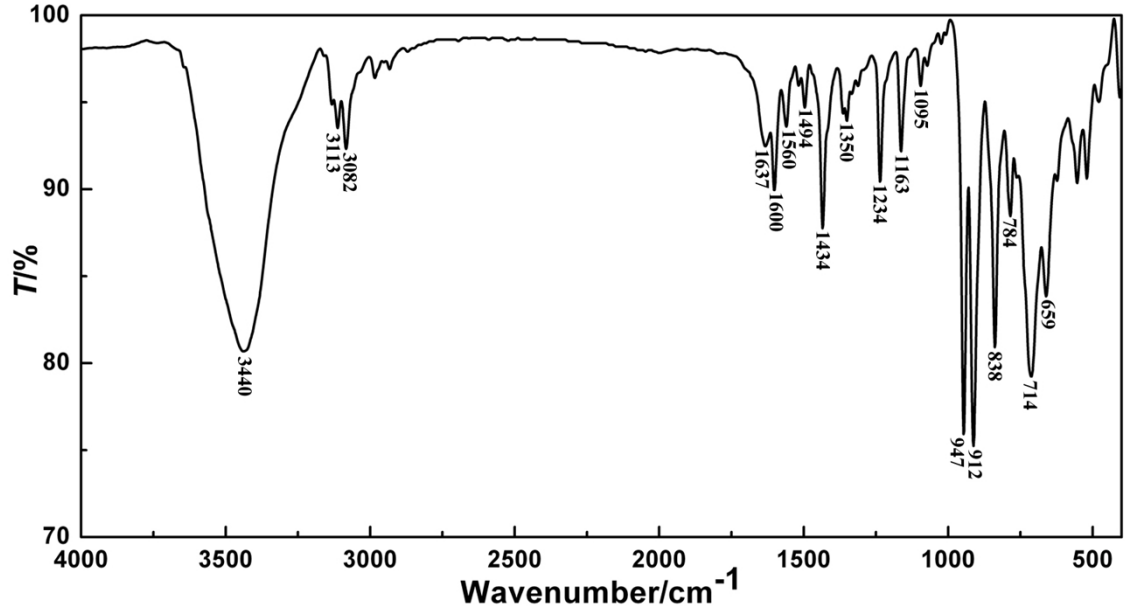


**Figure S29** IR spectrum of compound **7**.

**3.3** TG Analyses

The TG curve of compound **1** shows one weight loss step (Fig. S30). The whole weight loss of 43.48% occurring from 325 to 595 °C is mainly ascribed to the decomposition and loss of L*o* ligands in **1** (calcd. 43.76%).

The TG curve of compound **2** shows two continuous weight loss steps (Fig. S31). The first weight loss of 1.43 % in the temperature range of 75 ~ 145°C corresponds to the loss of eight lattice water molecules (calcd. 1.69%). The second weight loss of 36.85% occurring from 325 to 590 °C is mainly ascribed to the decomposition and loss of L*o* ligands (calcd. 36.78%). The whole weight loss of 38.28 % is in agreement with the calculated value 38.47%.

The TG curve of compound **3** (Fig. S32) shows the first weight loss of 1.82% in the temperature range of 75 ~ 120 °C corresponding to three lattice water molecules (calculated value 1.89%). The second weight loss of 37.51 % from 330 to 610 °C is ascribed to decomposition and loss of pzpy and L*o* ligands (calcd. 37.57%). The whole weight loss of 39.33% is in agreement with the calculated value 39.46%.

The TG curve of compound **4** also displays two continuous weight loss steps (Fig. S33). The first weight loss of 3.29 % in the temperature range of 85 ~ 140 °C corresponds to the loss of four coordinated water molecules and four lattice water molecules (calcd. 3.32%). The second weight loss in the range of 335 ~ 610 °C is 35.89% and attributed to the loss of L*p* ligands (calcd. 36.17%). The whole weight loss of 39.18 % is in agreement with the calculated value 39.49%.

The TG curve of compound **5** displays one weight loss steps (Fig. S34). The whole weight loss of 44.31% occurring from 320 to 620 °C is mainly attributed to the decomposition and loss of L*p* ligands in **5** (calcd. 44.66%).

The TG curve of compound **6** shows one weight loss steps (Fig. S35). The whole weight loss of 52.20% occurring from 330 to 630 °C is mainly ascribed to the decomposition and loss of L*p* ligands in **6** (calcd. 52.14%).

The TG curve of compound **7** displays one weight loss steps (Fig. S36). The whole weight loss of 41.85% occurring from 325 to 640 °C is mainly attributed to the decomposition and loss of L*p* ligands and bmin cation in **7** (calcd. 41.94%).

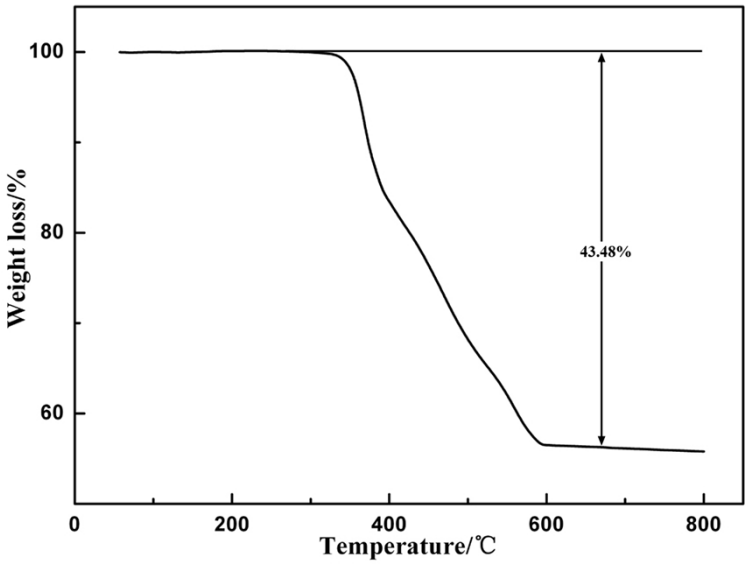


**Figure S30** TG curve of compound **1**.

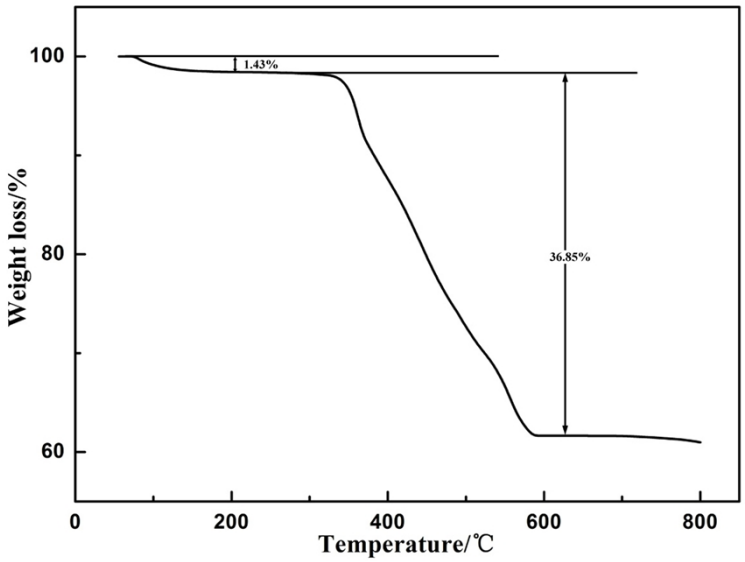


**Figure S31** TG curve of compound **2**.

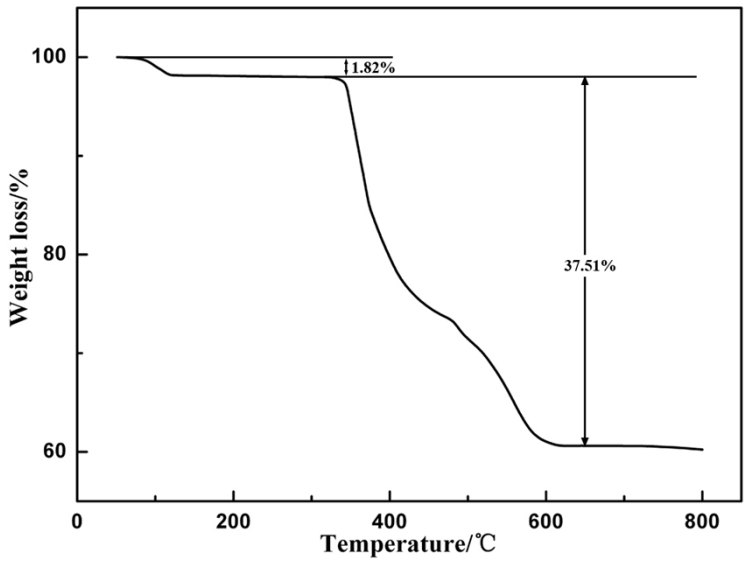


**Figure S32** TG curve of compound **3**.

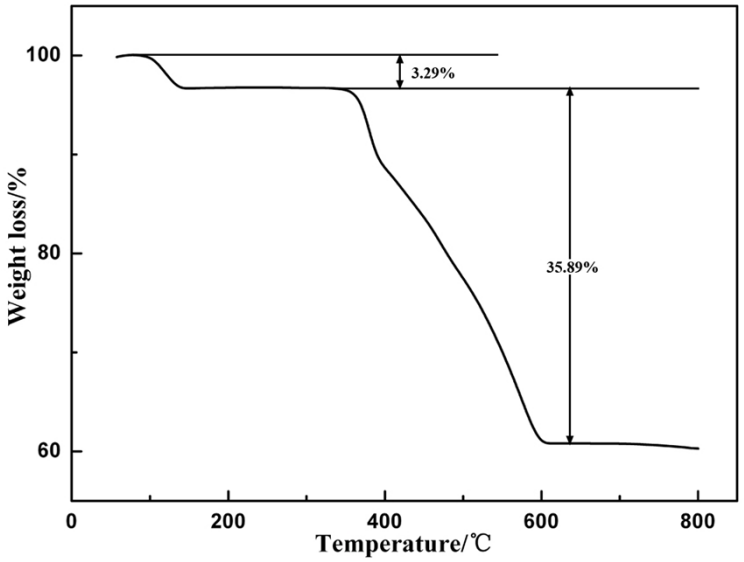


**Figure S33** TG curve of compound **4**.

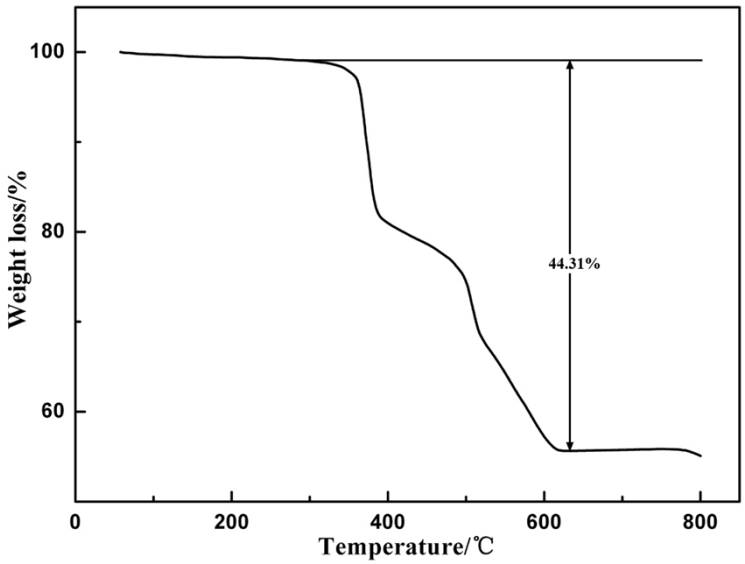


**Figure S34** TG curve of compound **5**.

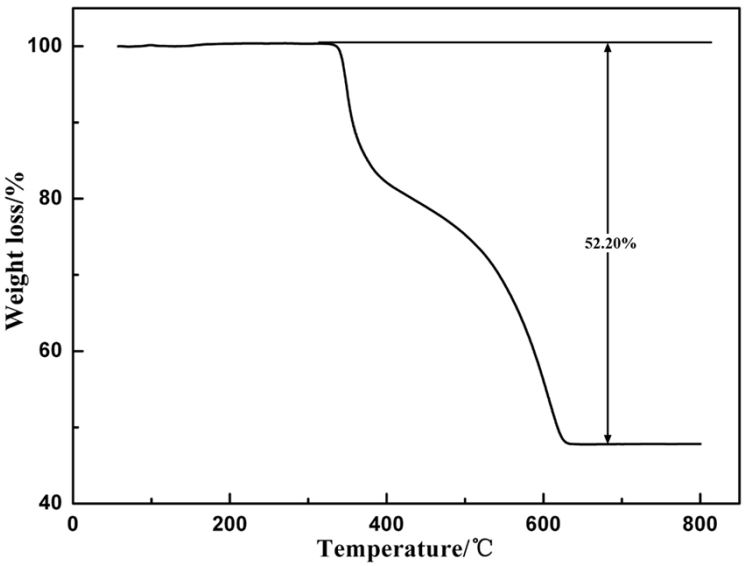


**Figure S35** TG curve of compound **6**.

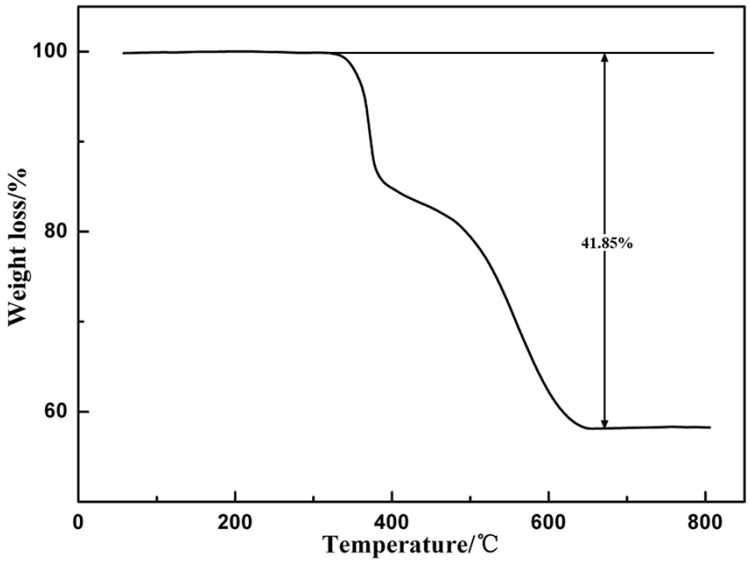


**Figure S36** TG curve of compound **7**.

**3.4** Powder X-ray diffractions

In order to check the phase purity of compounds **1**-**7**, the PXRD patterns of them were recorded at room temperature. As shown in Figs. S37-S43, the peak positions of simulated and experimental patterns of compounds **1**-**7** are in agreement with each other, indicating the good phase purity of them. The differences in intensity are owing to the preferred orientations of the crystalline powder samples.

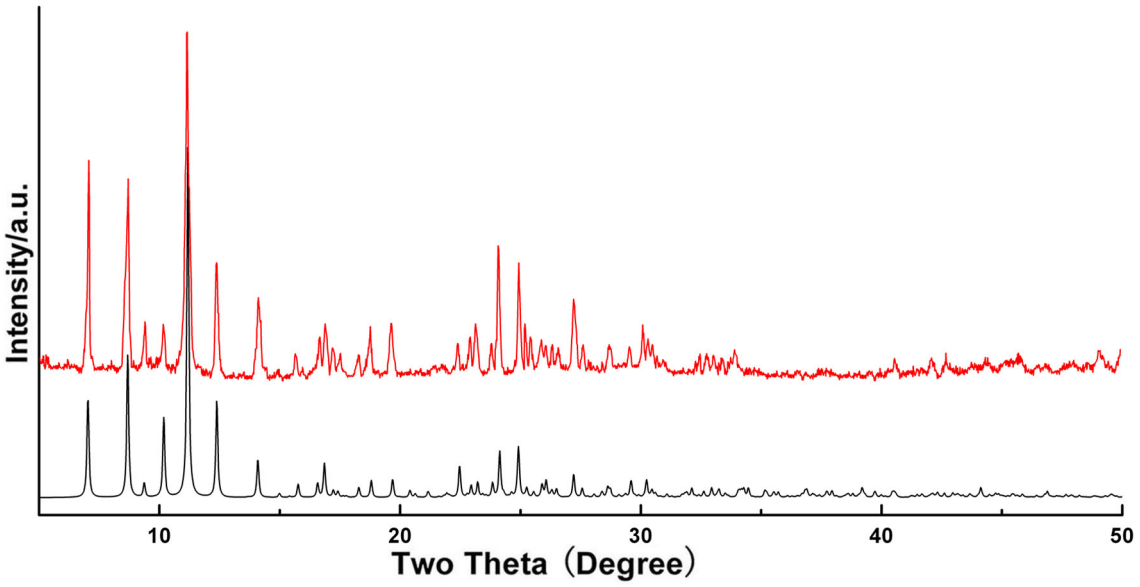


**Figure S37** Measured (red) and simulated (black) XRD patterns of compound **1**.

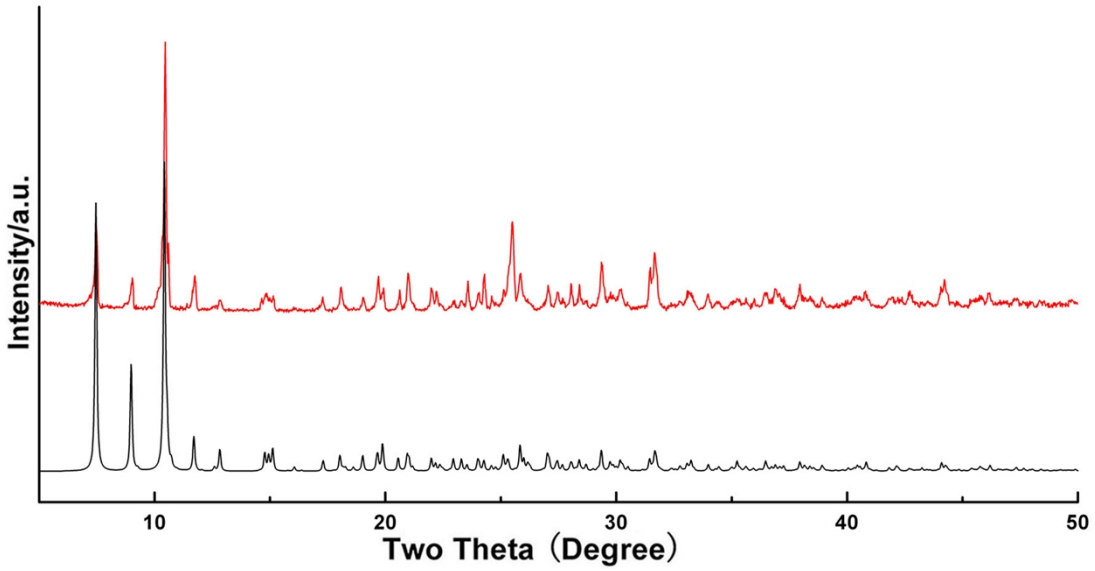


**Figure S38** Measured (red) and simulated (black) XRD patterns of compound **2**.

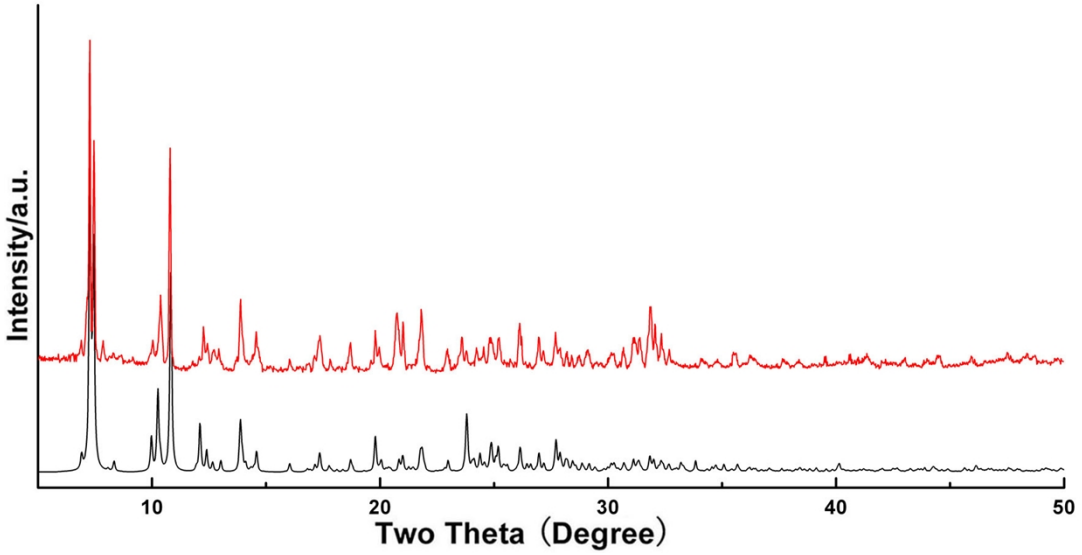


**Figure S39** Measured (red) and simulated (black) XRD patterns of compound **3**.

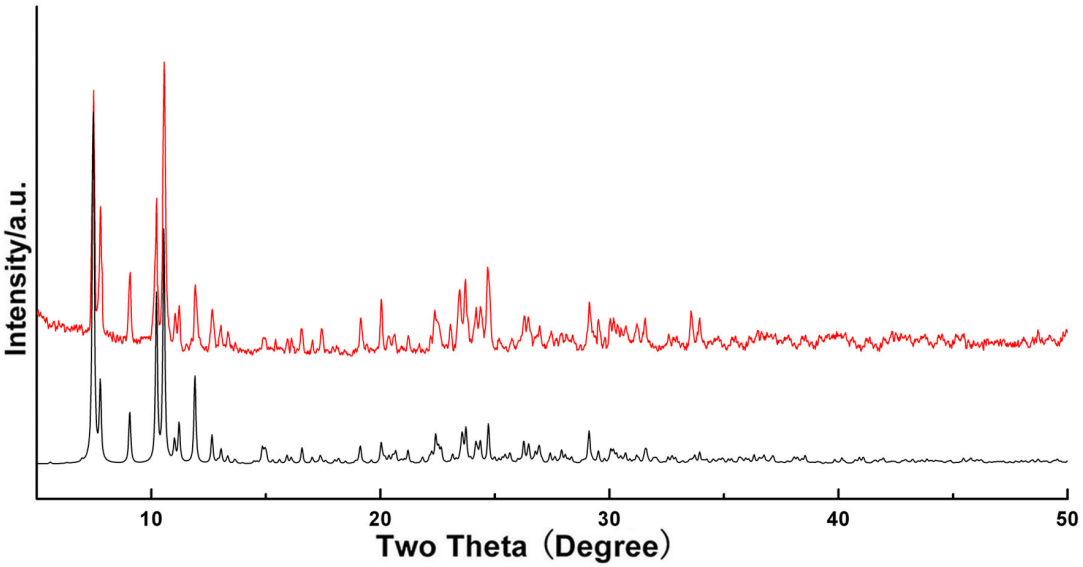


**Figure S40** Measured (red) and simulated (black) XRD patterns of compound **4**.

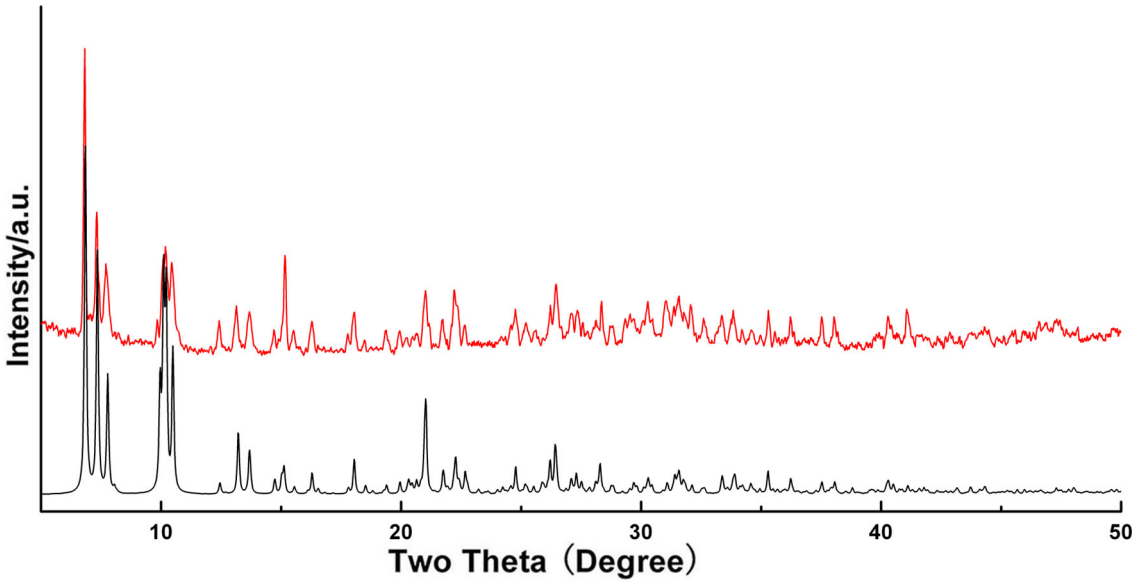


**Figure S41** Measured (red) and simulated (black) XRD patterns of compound **5**.

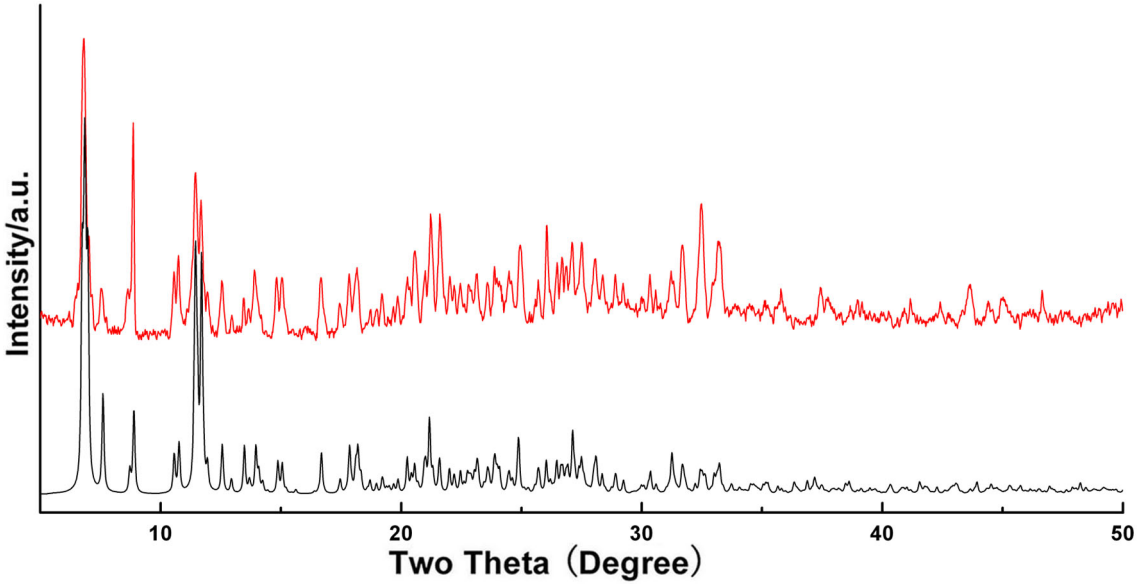


**Figure S42** Measured (red) and simulated (black) XRD patterns of compound **6**.

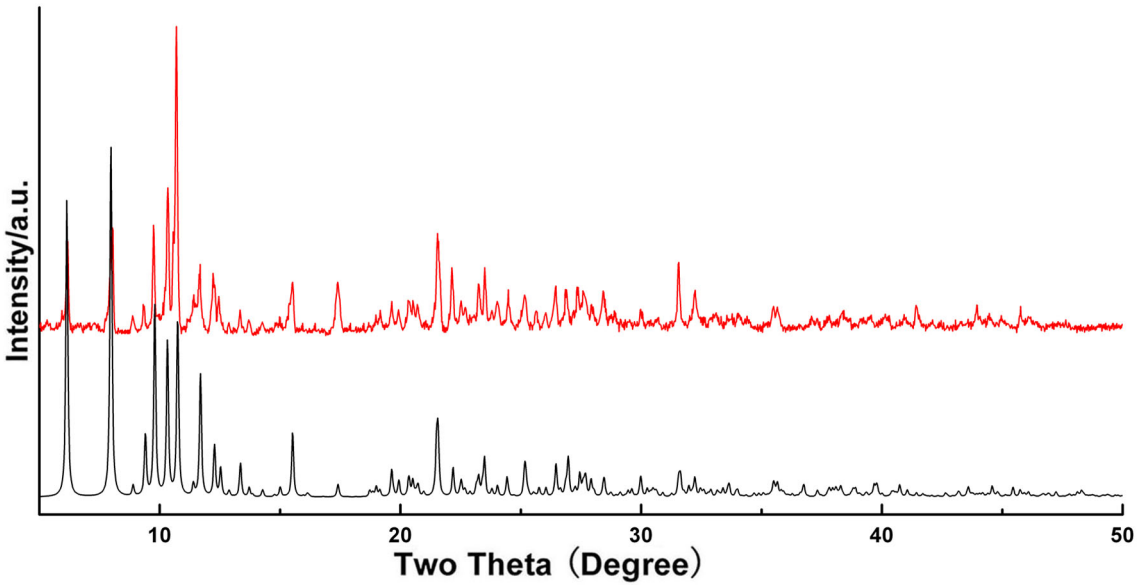


**Figure S43** Measured (red) and simulated (black) XRD patterns of compound **7**.